INTERDIFFUSION MEASUREMENTS IN THERMALLY CONTROLLED MICROCHANNEL USING INFRARED SPECTROSCOPIC IMAGING

Marine Garcia

Arts et Métiers Institute of Technology, CNRS, Université de Bordeaux, Bordeaux INP

Institut de Mécanique et d'Ingénierie (I2M), Bâtiment A11,

351 Cours de la Libération, 33405 Talence, France

Alain Sommier

CNRS, Arts et Métiers Institute of Technology, Université de Bordeaux, Bordeaux INP

Institut de Mécanique et d'Ingénierie (I2M), Bâtiment A11,

351 Cours de la Libération, 33405 Talence, France

Thomas Lafargue-Taller

CNRS, Arts et Métiers Institute of Technology, Université de Bordeaux, Bordeaux INP

Institut de Mécanique et d'Ingénierie (I2M), Bâtiment A11,

351 Cours de la Libération, 33405 Talence, France

Gérald Clisson

CNRS, Solvay, LOF, UMR 5258

178, avenue du Docteur Schweitzer,33608 Pessac, France

Jean-Christophe Batsale

Arts et Métiers Institute of Technology, CNRS, Université de Bordeaux, Bordeaux INP,

Institut de Mécanique et d'Ingénierie (I2M), Bâtiment A11,

351 Cours de la Libération, 33405 Talence, France

Stéphane Chevalier*

Arts et Métiers Institute of Technology, Université de Bordeaux, Bordeaux INP

Institut de Mécanique et d'Ingénierie (I2M), Bâtiment A11,

351 Cours de la Libération, 33405 Talence, France

June 30, 2023

*Corresponding Author: Prof. Stéphane Chevalier, stephane.chevalier@u-bordeaux.fr

ABSTRACT

In many applications, knowledge of the mass diffusivity coefficient is mandatory to optimize the design and operating conditions of microfluidic devices and chemical reactions. The literature reports few values due to limited techniques, and the impact of the fluid temperature is rarely taken into account when the diffusivity is measured. In this study, we present an imaging method to investigate and quantify the interdiffusion of two fluids in a microchannel under controlled temperatures. The experimental setup combines a thermally controlled microfluidic chip and a microscale infrared (IR) spectroscopy imaging technique. The mass diffusivity of formic acid (HCOOH) in sulfuric acid (H_2SO_4) was measured from room temperature to 50° C to demonstrate the performance of the setup. This work offers a rapid tool and a methodology for accurate contactless interdiffusion measurements in thermally controlled T-shape reactors applicable a large set of chemicals.

Nomenclature

Roman letters

A		absorbance
a	mm	diffusion length
C	mol/L	concentration
C_n		normalized concentration
D	mm^2/s	diffusion coefficient
H	mm	PDMS stamp height
h	mm	channel height
L	mm	channel length
l_c	mm	channel width
M	mol/L	molar concentration
Pe		Peclet number
T	°C	temperature
v	m/s	mean velocity

Greek letters

α	mm^2	diffusion cone surface
γ		channel aspect ratio
λ	µm	wavelength
μ	$M^{-1}.mm^{-1}$	absorptivity coefficient

1 Introduction

Microfluidics are used in many applications to better understand processes at the microscale, such as cancer cell extravasation [1], the kinetics of chemical reactions [2, 3] or diffusion of a solute [4]. The main advantages of using microscale devices relies on precise control of the experimental conditions (pressure, flow rate, channel geometry), low reagent volumes and the increased sensitivity of the analysis [5]. Moreover, at this scale, phenomena such as heat and mass transport are enhanced. In the field of chemistry the transport phenomena play a crutial role. For example, in chemical reactors, diffusion occurring at the fluid interface influences the efficiency of the reaction. In microfluidic fuel cells (MFCs), mass transport phenomena affect the MFC limiting current [6] and cell geometry [7, 8]. Hence, a quantitative analysis of the diffusion coefficient appears to be necessary for understanding, scaling and modeling complex systems with one of several fluid interfaces. However, few studies in the literature report mass transfer measurements, especially for aqueous systems [9, 10]. Investigating diffusion for aqueous species at various temperatures is reported even less frequently despite the diffusion coefficient being significantly affected by the fluid temperature.

To experimentally investigate the mass transfer in a microchannel, several optical imaging systems have been reported [11]. Two dimentional (2D) imaging techniques based on fluorescence emission can be used to investigate in situ parameters such as viscosity [12] or diffusion coefficients. In the work presented by Culbertson et al.[13], solutions with fluorescent particles such as rhodamine 6G where used to observe the mass transfer. They managed to determine the diffusion coefficient by measuring the fluorescent peak variance over time. This technique can be easily implemented since it does not require a complex light source such as a Fourier transform IR (FTIR) spectrometer. However, this technique is limited to fluorescent media and by photobleaching which imposes a short exposure time. Another method used for studying mass transfer found in the literature is Raman confocal microscopy. Salmon et al. [14] used it to measure the molar fraction of species in a solution and to estimate the diffusion coefficient of a reactant. Raman spectroscopy is a highly selective chemical imaging technique, but it is a point-by-point measurement and suffers from long acquisition times. As integration times range from milliseconds to minutes [15], single measurements can take at least one hour.

Fluorescence and Raman spectroscopy are limited techniques when it comes to study multiples chemicals especially in the case of aqueous solutions [16]. Fluorescence techniques are sensitive but limited to molecules linked to a fluorophore and Raman spectroscopy is very selective but suffer from lack of sensitivity [17]. To study mass transport phenomena, infrared spectroscopic techniques such as mid infrared (MIR) or near infrared (NIR) spectroscopy can be considered [18]. To measure both temperature and concentration fields, Yamashita et al. have proposed a method based on a NIR absorption imaging technique [19]. A NIR camera was used to measure the transmitted light at two specific wavelengths λ_1 =1935 nm and λ_2 =1905 nm. A good agreement to values reported in the literature is presented but the monochromatic light restricts the analysis to one component. This issue can be overcome by using FTIR spectroscopy, since FTIR spectroscopic techniques measure molar concentration of several species from the multispectral absorbance [18]. Chan et al used a FTIR spectroscopic imaging technique to study the distribution of different chemicals in

microfluidic devices [20]. This technique has been very popular for studying chemical reactions such as acid-base reactions [16, 21]. From the images generated by these methods, these authors were able to give quantitative 2D concentration fields along the channel. FTIR spectroscopy is also used for pharmaceutical investigations. Ewing et al. used ATR-FTIR spectroscopy to study the release and the behavior of drug at specific pH and flow rate [22]. Other recent work using FTIR imaging techniques are described in Ref. [17]. These studies are also prime of interest because they demonstrate that transmission IR spectroscopy is possible even through several tens of micrometers of water in the mid-IR wavelength range. Thus, by extending this technique, it appears to be highly promising for quantitatively investigating the mass diffusion process in aqueous species.

To have a complete understanding of the diffusion process, the effect of the temperature has to be taken into account since the diffusion coefficient is temperature dependent [23].In the case of microfluidic chips, heating is usually achieved using an external device such as a Peltier module placed underneath a microchip. Annular geometries can be used to allow light transmission in the sample [19], but the substrate must be carefully chosen to ensure a homogeneous temperature field. For commonly used substrates that have a poor thermal conductivity, such as glass, thermocouples appear necessary to control the fluid temperature. However, due to the size of the thermocouple (several hundreds of micrometers, at best), they can cause local perturbations in the heat field when placed close to the micrometric channel [24]. To overcome this problem, Casquillas et al. [25] used a Peltier module to heat or cool the fluids from 5° C to 45° C before they were injected into the microfluidic cell (preheated or cooled down liquids). Since no elements were placed underneath, the chip was associated with an oil immersion objective lens for live cell imaging. Other methods for controlling the chip temperature can be found in the literature, such as thin film heating, Joules heating or microwave dielectric heating [26]. However, as reported by several authors, temperature measurement and homogeneous temperature profiles are not trivial to master and control.

In this study, we propose a multispectral imaging technique for quasi real-time measurements. In fact, multispectral acquisition can be completed in less than 15 s [20]. This method is based on IR transmission spectroscopy to measure the mass transfer in a T-shape microchannel. The chemical concentration fields of each species in a microfluidic channel are obtained using an FTIR imaging technique associated with the Beer-Lambert law. The mass transfer estimation is performed through an analytical inverse method based on Fick's equation and a least square regression that makes the processing of the images as fast as a few seconds. To control temperature, a thermistor associated with a heating resistance is integrated into the experimental setup to control the temperature of the chip from room temperature to 50 °C. The design and material choice for microfluidic cell have been adapted to reduce heat losses, to achieve a homogeneous temperature field and to maximize the IR transmitted light through the chip.

2 Materials and method

2.1 Fabrication of the microfluidic channel

The materials were carefully chosen to control the dimensions of the microchannel and to obtain a device that is compatible with IR spectroscopy in the 2-5 μm wavelength range. In fact, IR spectroscopy is limited by the optical path, the absorption of water and the absorption of the materials used to fabricate the cell. To overcome this problem, PDMS is chosen as a material to fabricate the microchannel. PDMS can be used in IR since it is semitransparent in this range [27]. Additionally, since photolithography techniques are used to obtain the PDMS stamp, dimensions of a few micrometers can be achieved. Hence, by reducing the channel height to a few micrometers as well as the thickness of the PDMS stamp, the quantity of transmitted IR light is increased. Microchannels made in PDMS are usually bound on glass substrates such as borofloat wafers. However, such glass wafers suffer from a very low thermal conductivity ($\lambda \sim 1.2$ W/m/K), which is disadvantageous for thermal control. To overcome this problem, a silicon double side polished wafer is used as a substrate. The use of silicon wafers presents two main advantages. First, they have better light transmission characteristics than glass in the IR range, and the thermal conductivity is very high ($\lambda \sim 149$ W/m/K). Therefore, a silicon wafer appears to be the most convenient substrate to combine transmitted IR imaging spectroscopy and uniform chip temperature.

A single T-shaped microfluidic channel is fabricated using a standard photolithography method illustrated in Figure 1. A negative photoresist resin is spin coated on a silicon wafer a), covered with a photomask and exposed to UV light b) before being submerged in a PGMEA solution for development c). The obtained mold is placed in a Petri dish and coated with 5 mm of PDMS d). After curing, the PDMS is peeled off the mold e) and is hole-punched to create two inlets and one outlet. A double-side polished silicon wafer is used as the substrate for the final device. The PDMS and the silicon substrate are plasma activated to bond the PDMS to the substrate f). The PDMS stamps height H is 5 mm, the microchannel height h is $22\,\mu$m and the width l_c is 2 mm. Regarding the aspect ratio of the microchannel ($l_c/h \sim 90$), one can assume the channel and the flow to be 2D. This assumption is verified in section 2.4.

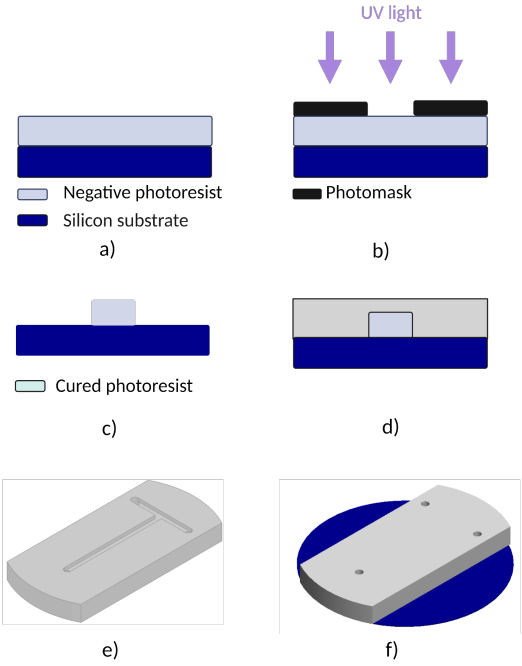

Figure 1: Schematic of the fabrication process used to produce a microfluidic T channel cell. Each step is labeled from a) to f).

2.2 Experimental setup

To thermally control the microchannel, the microfluidic cell is placed on an annular custom-made nickel thermistor deposited on a thin heating resistor (Captec). Such a system is capable of controlling the temperature up to 80 °C ± 0.1°C. The contact between the thermistor and the cell is ensured by a mechanical compression system (see Figure 2a)) made of an insulating support (machined Bakelite) and two clamps. The heating resistor is connected to a DC power supply, and an acquisition card is used to measure the electrical resistance of the nickel probe. A LabVIEW algorithm is used to convert the resistance of the nickel probe in temperature and then acts as a PID controller to determine the current that the power supply has to deliver to reach and maintain the temperature set point.

Figure 2 c) presents the plate assembly integrated with the experimental setup, which combines the spectroscopic imaging technique and temperature control of the sample. In Figure 2 c), an FTIR spectrometer (Thermo Fisher Nicolet IS50R) is used as the IR source to perform multispectral absorbance measurements. A mirror is used to redirect the beam through the cell, and the attenuated beam is captured by the camera. An FLIR SC7000 camera with an InSb focal plane array in the range of 2-5 μm is used with a microscopic objective. The imaging system has a spatial resolution of

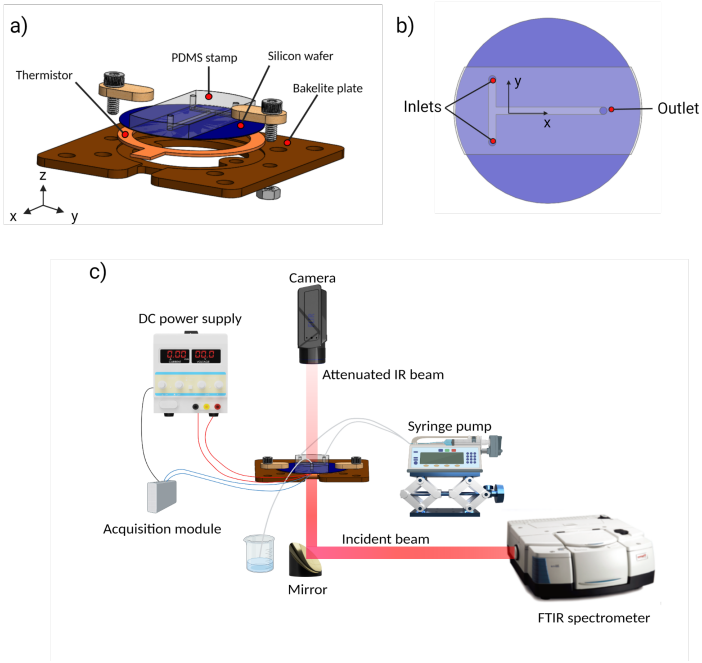

Figure 2: a) 3D view of the cell with the associated support containing the thermistor and the Bakelite plate. b) Schematic of the microfluidic cell with the coordinate system used. c) Experimental setup used for visualization of the multispectral absorbance fields in the microchannel.

$14\,\mu\mathrm{m/pxl}$. The camera and spectrometer settings and controls are defined following the methodology described in Chevalier et al. [28].

2.3 Absorbance measurements

The experimental setup is used to study the diffusion of formic acid (HCOOH) in sulfuric acid (H_2SO_4). Formic acid is an interesting chemical since it is used in various sectors, such as pharmaceuticals, feed additives or even as a source of hydrogen and carbon monoxide [29], and it has a temperature-dependent diffusivity. It must be mentioned that formic acid is a colorless product that is completely transparent in the visible range, but it shows a clear absorption spectrum in the IR range. The method described in this study remains valid for all chemicals with similar optical properties.

In the experiments, two aqueous solutions are prepared: the first one is a solution S1 containing 0.5 M of H_2SO_4, and the second solution S2 is prepared by mixing 1 M H_2SO_4 with 4 M HCOOH in a 1:1 ratio to reach a final concentration of 0.5 M H_2SO_4 + 2 M HCOOH. The fluids flow for several minutes to evacuate bubbles and to reach steady-state. Subsequently, two sets of images are acquired: in the first experiment, only S1 flows in the channel. The resulting image is defined as the background. In the second experiment, there is a coflow of S1 and S2 in the channel defined as the sample . The transmission spectrum for every pixel is recorded by the FTIR imaging platform to compute the

multispectral absorbance using the Beer-Lambert law. The Beer Lambert Law that relates light intensity variations with the fluid concentration [30] is

$$A(x, y, \lambda, C) = -\log\left(\frac{I(x, y, \lambda, C)}{I_0(x, y, \lambda)}\right), \tag{1}$$

where A is the multispectral absorbance, I_0 is the background spectrum, and I is the spectrum with S1 and S2 flowing in the channel. I and I_0 are acquired over an x by y area for a wavelength range λ. C stands for the concentration of formic acid. To observe the rate of HCOOH diffusion into (H_2SO_4), I_0 is the recorded transmitted signal with only H_2SO_4 flowing in the chip.

The concentration of formic acid is related to absorbance through

$$A(x, y, \lambda, C) = \mu(\lambda)\, C(x, y), \tag{2}$$

where μ is the absorptivity coefficient ($M^{-1}.mm^{-1}$). It was measured to 4.38 $M^{-1}.mm^{-1}$ for formic acid at 4 µm, see the section Absorptivity of formic acid reported in supplementary information. To increase the signal-to-noise ratio (SNR), the absorbance is integrated over a spectral range as

$$A_{int}(x, y, C) = \int_{\lambda_1}^{\lambda_2} \mu(\lambda)\, C(x, y)\, d(\lambda). \tag{3}$$

Eq. 4 gives a relation between the absorbance and the concentration that is no more dependent on the wavelength

$$A_{int}(x, y, C) = k\, C(x, y), \tag{4}$$

with k is the integrated absorptivity coefficient. The integrated absorbance is then normalized between 0 and 1 to obtain the normalized concentration through

$$C_n = \frac{A_{int}(x, y, C) - \min(A_{int}(x, y, C))}{\max(A_{int}(x, y, C)) - \min(A_{int}(x, y, C))}, \tag{5}$$

An important point to note in Eq. 5 is that the normalization operation gives a direct relation between absorbance and concentration; thus, absorptivity calibration is no longer required. Such an advantage makes the measurements much faster than other techniques such as fluorescence, which requires calibration to link the fluorescence intensity to the molar concentration [31].

2.4 Interdiffusion model

The geometry of a laminar microfluidic electrochemical chip is schemed in Figure 2 b). A large width to height aspect ratio channel was designed to ensure a Reynolds number < 1 leading to a laminar flow. In the case of a diluted solution (which is frequent with aqueous solutions), the Fickian diffusion in steady state can be used to describe the transport of

the species concentration in a microchannel as

$$\nabla \cdot (-D\overrightarrow{\nabla} C + \vec{v}C) = 0. \tag{6}$$

D is the mass diffusivity (mm^2/s), $\vec{v}$ is the velocity vector (mm/s) and C is the molar concentration (mol/L). Equation (6) can be simplified using the following assumptions: D is considered independent of the concentration and no chemical interaction between fluids occurs. The fluids used are highly diluted leading to similar viscosity and density. Since the fluids are injected with same flow rate, the fluid-fluid interface is centered in the middle of the channel and the velocity profile is homogenous. In the x-direction, the Peclet number Pe=2x10^3 is large enough to assume that the convective mass transport is dominant over diffusion $\partial^2 c/\partial x^2 \approx 0$. Regarding the geometry of the channel, the velocity profile is uniform in the y-direction far from the channel walls, so we assume $\vec{v} = v$ with $v = q_v/(hl_c)$. Finally, given the high aspect ratio of the channel $\gamma = l_c/h \gg 1$, the molar gradient in z-direction can be neglected. The validity of those assumptions is evaluated in the supplementary information and compared to a 3D numerical model solved without any assumptions. Therefore, Equation 6 can be rewritten in the 2D case as:

$$v\frac{\partial \bar{C}}{\partial x} = D\frac{\partial^2 \bar{C}}{\partial y^2}, \tag{7}$$

where v is the average velocity, and $\bar{C}$ the average concentration measured from the absorbance $\bar{C}(x,y) = \frac{1}{h}\int_0^h C(x,y,z)dz \approx C(x,y)$, see section 2.3. We assumed a semi-infinite field in the x-direction and the boundary conditions are $\frac{\partial \bar{C}}{\partial y}|_{y=0} = 0$ and $\bar{C}(x, y \to \infty) = C_0$. A solution using the normalized concentration (see Equation 5) to the previous equation can be found as [32, 14]:

$$\bar{C_n}(x,y) = \frac{1}{2}\left(1 + \text{erf}\left(\frac{y - y_o}{2(\sqrt{\frac{D(x-x_0)}{v}})}\right)\right), \tag{8}$$

y_0 and x_0 are two constants (in mm) related to the reactant interface and diffusion onset position, respectively.The diffusion length $a(x)$ in millimeters can be defined as:

$$a(x) = \sqrt{\frac{D(x - x_0)}{v}} \tag{9}$$

3 Results and discussion

3.1 Validations of the methodology

Limits of the analytical solution

In order to validate the analytical solution proposed in Equation 7, and all the assumptions made in the methodology section, a comparison with a numerical model was done. Equation 6 was solved numerically in 3D without assumptions for a microfluidic channel with the same dimensions as the one used experimentally. The results of the numerical model

are given in supplementary information section 2.

In Figure 3 the analytical solution (Equation 8) for a range of x position is compared to the concentration profile computed numerically at the same position.

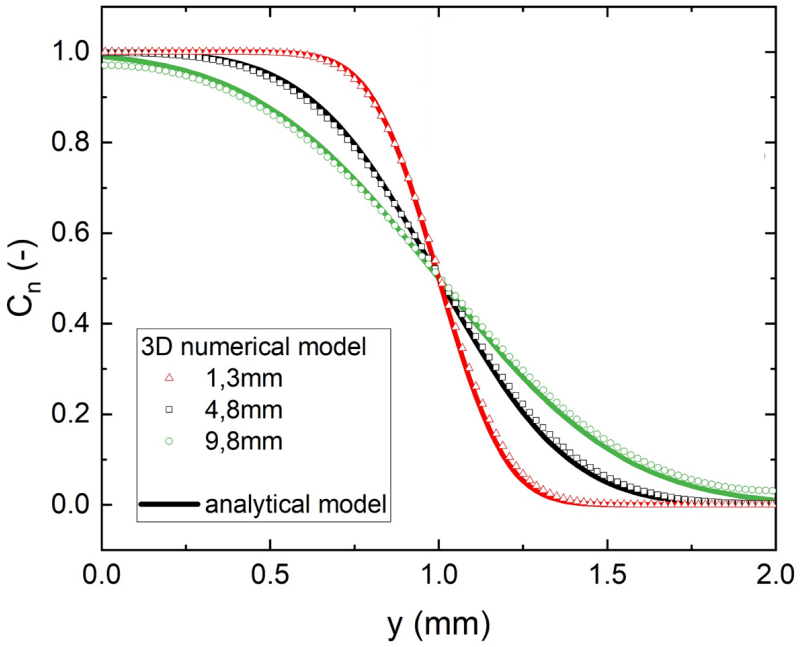

Figure 3: Average concentration profiles for a range of x-positions computed from the analytical model and the numerical model.

The excellent agreement between the models validates the use of a analytical model to estimate the mass diffusivity in the range of operating conditions used in this study, i.e. a total flow rate of 1 µl/min and a diffusivity in the range of 2×10^{-3} mm^2/s. For the profiles obtained at $x > 5$ mm, a small deviation can be observed close to the wall, i.e. $y = 0$ and $y = l_c$ where the semi-infinite assumption is no longer valid. Thus, this numerical study enables to set the limit of the use of the proposed methodology.

Thermal control of the microchannel

Experiements are performed with the fluids not preheated before being injected into the microchannel, which may induce thermal gradients in the chip. Thus, before carrying out the concentration field measurements, the temperature homogeneity of the microfluidic chip is checked for a range of flow rates. For this purpose, the same experimental setup as the one presented in Figure 2.b) is used but with the FTIR spectrometer shut off. In this configuration, the camera is used to perform IR thermography, which consists of measuring the IR emission field at the surface of a

system [33]. To obtain a temperature field, calibration of the IR camera was performed according to the methodology reported in Lafargue-Tallet et al. [34]. To observe the temperature field in the cell, a microfluidic chip identical to the one presented in Figure 1 is used, but with the rear face (the face without the PDMS stamp) painted in black to be assimilated to a black body surface. The black rear face is placed facing the camera, and the tubing is connected to flow fluids in the cell. The chip is heated without fluids flowing in, and after 10 min, the temperature of the rear face is recorded by the camera. Hence, a nonperturbed temperature map of the rear face T_0 is obtained. Fluids are then flowed in the microchannel at a given flow rate for 10 min, and the chip rear face temperature T is measured again. The same protocol was repeated for flow rates ranging from 0.5 to 100 $\mu\mathrm{l}/\mathrm{min}$. The variation in the temperature field $\Delta T = T_0 - T$ of the rear face is presented in Figure 4 with a temperature setpoint of 40 °C.

Figure 4 a) shows that with a flow rate of $100\,\mu\mathrm{l}/\mathrm{min}$ at both inlets, a clear temperature gradient is observed around the channel. The maximum temperature difference is estimated to be approximately 1 °C and is located close to the inlets. Figure 4 b) shows that at the lowest flow rate, the temperature is completely homogeneous since only noise is observed at approximately 0.02 °C. These results show that the flow rate is a key parameter to achieve accurate control of the temperature without preheating the fluids. At a high flow rate ($100\,\mu\mathrm{l}/\mathrm{min}$), the residence time of the fluid to go from the inlet to the main channel is not enough to heat the fluid (half a second), causing a thermal gradient. Conversely, for a flow rate of $1\,\mu\mathrm{l}/\mathrm{min}$, the residence time to reach the main channel increases to almost 30 s. At this low flow rate, only noise is measured, and the temperature field is homogeneous at the surface of the chip. Thus, this result validates the thermal control of the proposed setup as long as the flow rate is kept on the order of $1\,\mu\mathrm{l}/\mathrm{min}$. The temperature standard deviation in the main channel (white line in Figure 4(b)) is not larger than 0.18 °C at 40 °C.

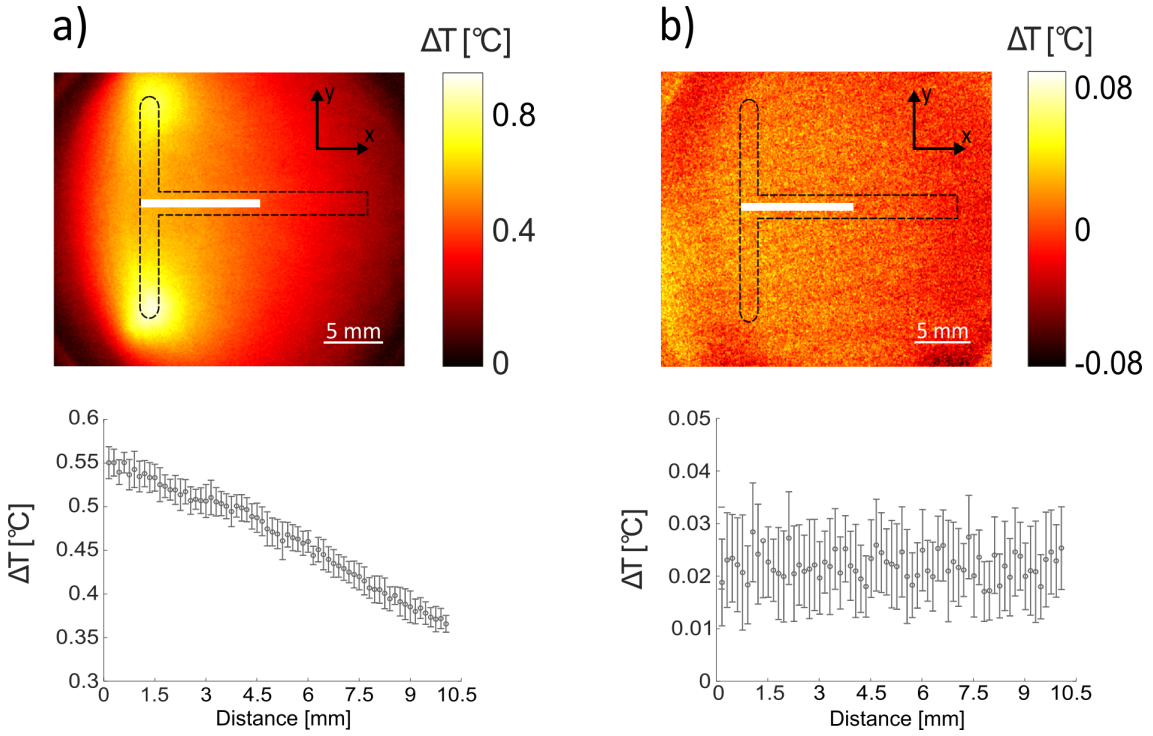

Figure 4: Temperature field variations measured on the surface of the chip rear face at a) $100\,\mu l/min$ and b) $1\,\mu l/min$ at each inlet. Relative temperature profiles indicated by the white lines are plotted under each case.

3.2 Normalized concentration fields

Prior estimating the diffusion of formic acid in sulfuric acid, the experimental setup and the methodology were tested for the known case of the diffusion of formic acid in deionized water. The diffusion coefficient for this case was found to be D=(1.36 ± 0.15) x10−3 mm²/s. This value for the computed diffusion coefficient is comparable to the values reported in literature (1.49×10^{-3} mm^2/s [35], 1.46×10^{-3} mm^2/s) [36] and validates the experimental setup and the proposed method. More details about the results are given in the supplementary information section 3.

In the following experiment, water is replaced by sulfuric acid in order to study the diffusion of formic acid in sulfuric acid. Experiments are performed at room temperature (25° C), to 40° C and 50° C. A flow rate of 0.5 µl/min is imposed on both syringes for 5 min before starting the measurement. The spectra of the stream containing only HCOOH+H_2SO_4 and the stream containing only H_2SO_4 are first measured. As shown in Figure 5, sulfuric acid and formic acid have a very similar spectral signature in the camera IR range. We can see that it is not possible to distinguish formic acid from sulfuric acid and that only variation in the transmitted signal intensity is observed. Thus, careful signal processing is needed to convert the change in transmission light into normalized concentration fields, as can be seen Figure 5. This was achieved by integrating the spectra in the range indicated by the dashed rectangle in Figure 5, i.e., 3.9-4.3 µm.

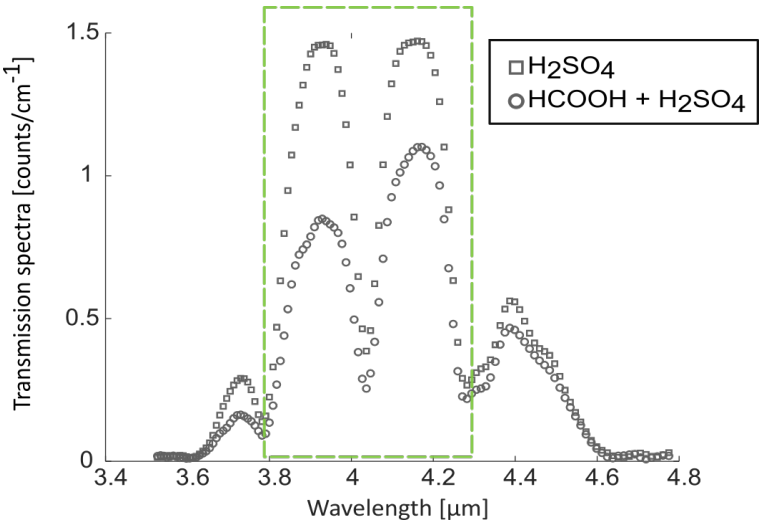

Figure 5: Spectra of the stream containing HCOOH+H_2SO_4 and the stream with H_2SO_4 only. The spectra are computed using the experimental data. Only the data in the green rectangle (dashed line) are used in the processing.

From the signal processing described in Section 2.3, the SNR is calculated to assess the performance of the measurements. It is defined by dividing the relative absorbance of the stream containing HCOOH+H_2SO_4 by the stream containing only H_2SO_4. Using a monochromatic absorbance, (wavelength of $4.1\,\mu\mathrm{m}$) where the relative absorbance of formic acid is maximized, the SNR is 10. Integration of the signal over the spectral range from Figure 5 increases the SNR to 100. The value of the SNR is then used to select the wavelength range for integration by choosing the spectral range which gives the highest SNR. Hence, this method significantly increases the SNR, allowing a better estimation of the diffusion coefficient than without integration. In many other chemical processes, the spectral signature between similar products can be identical. Using the change in transmitted light as proposed in this study enables an accurate measurement of the normalized concentration. Such a result would not have been possible using ATR spectroscopy, for example.

Figure 6b) presents the normalized absorbance profiles plotted for three different x positions. A change in slope is observed as the fluid flows toward the end of the channel. The slope change between the red curve and the green curve corresponds to the enlargement of the diffusion cone. This phenomenon indicates that diffusion along the y-direction occurs and confirms that it is possible to determine the diffusion coefficient using the absorbance profiles measured from room temperature to 50 °C. This maximum temperature was chosen to avoid any outgassing process as soon as the fluid temperature increases. Solutions for reaching temperatures above 50 °C can be found in the literature [37, 38], but this implies a more complicated microchannel design including degassing chambers.

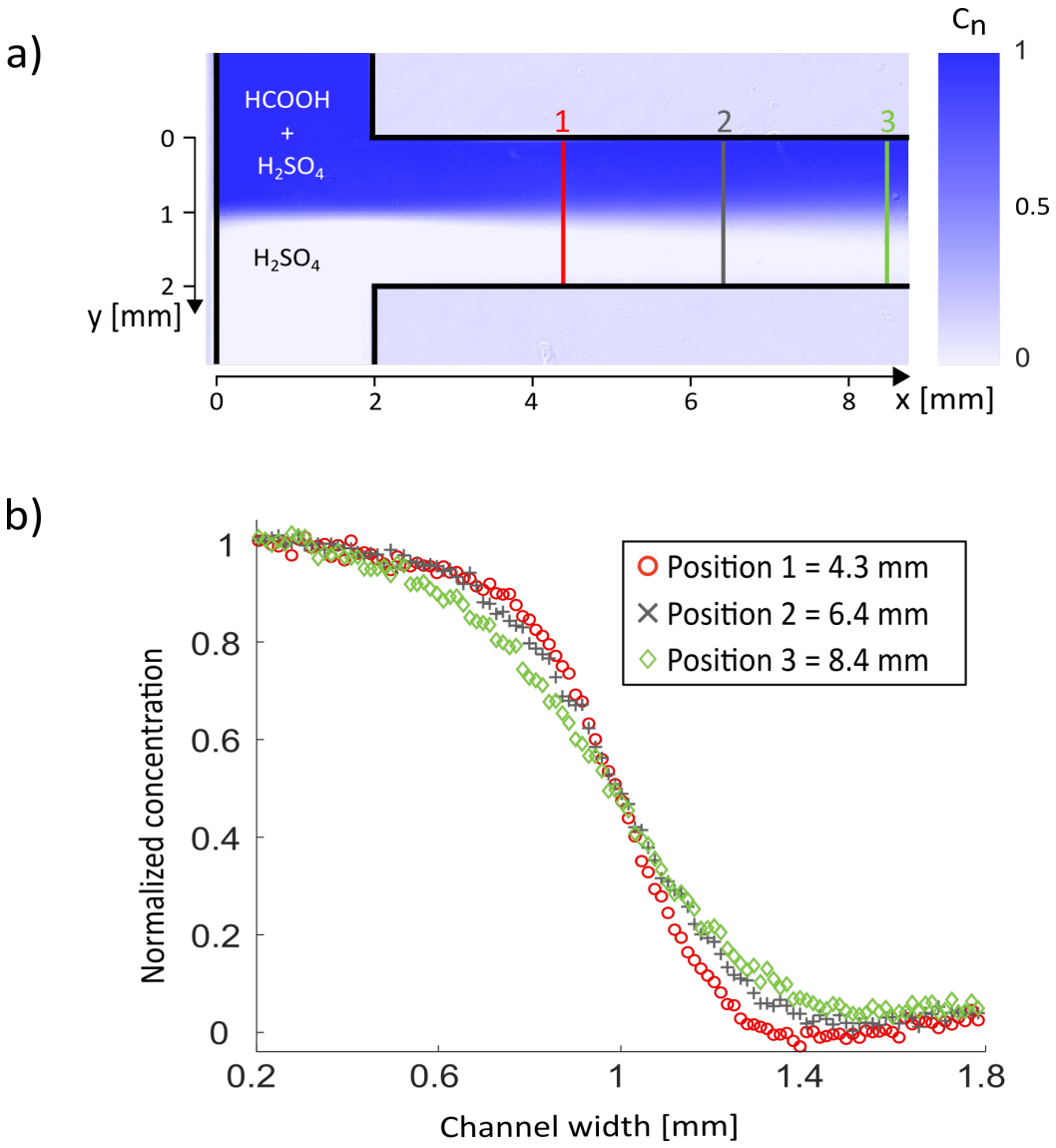

Figure 6: a) Normalized concentration fields of formic acid. The temperature was set to 40 °C, and the flow rate was $0.5\,\mu l/min$ at both inlets. b) Profiles of the normalized concentration at different positions in the main channel. Positions are labeled with reference to x=0 in the channel.

3.3 Determining of the diffusion coefficient

From the normalized absorbance of formic acid, the two linear regressions described in the supplementary informations section 4 are applied to compute D. The analytical solution given by the model permits to compute the standard deviation at each step using uncertainty propagation. The standard deviation values are then used to apply the weighted least squares linear regression on the dataset and to determine the mass diffusivity D in mm^2/s. The results of the weighted least squares linear regression for each temperature are presented in Figure 7.

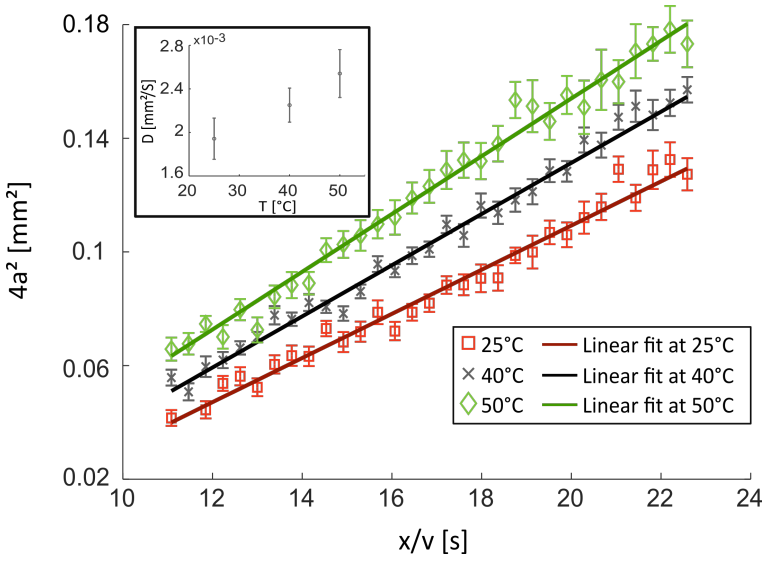

Figure 7: Plot of the computed coefficient $4a^2$ as a function of the ratio x/v for different temperatures. Solid lines show the linear regression fit of the data. Inset: estimated D in mm^2/s vs. the temperature.

Figure 7 displays the result of the second linear regression (details are provided in supplementary information section 4) used to compute the diffusion coefficient i.e., $4a^2$, as a function of x/v. When the temperature increases, the slope increases, leading to higher mass diffusivity. Table 1] displays the computed values of D.

T [°C]	D x 10^3[mm^2/s]
Room temperature	1.94 ± 0.19
40 ± 0.18	2.25 ± 0.16
50 ± 0.15	2.54 ± 0.22

Table 1: Computed values of the diffusion coefficient D

At 50 °C, D is 1.3 times higher than at 25 °C, this trend is also found in litterature [23], [39],[19] and confirms the sensitivity of D with temperature. To evaluate the fidelity of the model, a quantitative comparaison between the model using the computed D and the data is presented in the supplementary information section 5.

The study has presented results using formic acid, but this technique can be extended to more complex phenomena like diffusion coefficients concentration dependent. Such diffusion coefficients can be found in colloidal suspensions [40], solvent-polymer systems [41] or even aqueous binary mixtures [42]. The current limiting factor of the proposed setup is the choice of the compounds which need to have a spectral signatures ranging from 2 to 5 µm. Nevertheless, large spectral range detector may solve this limitation [43].

The region of interest used to study the mass transport is also essential to achieve precise measurements. Image acquisition must be performed on a region where the diffusion cone is well establish and large enough. Moreover, the concentration of the solutions must be carefully chosen to ensure a sufficient SNR to perform measurements.

Taking into account those recommendation, the proposed method leads to a relatively accurate measurements (see the error bar in the insert of Figure 7, or the reported values in Table 1). The diffusivity values were measured with less than 10% relative error with a temperature control of ± 0.18°C. The good model prediction and the low unbiased residue distribution (lower than 5% of error) presented in the supplementary information Figure S9 also strengthened the accuracy of the measurement performed. The experimental data validates setup and methodology reported in the present paper.

4 Conclusion

A novel imaging method to quantitatively study mass transport phenomena is reported in this work under controlled thermal conditions. This was achieved by using a microfluidic chip that uses a silicon wafer and a heating system to control the temperature of the device while maintaining IR transparency in the desired wavelength range. Integrating a thermistor allowed us to control the experimental conditions to study the mass transport for temperatures up to 50 °C. A thorough check of the temperature homogeneity was also carried out. It was shown that using no preheated fluid at a low flow rate in the microfluidic channel does not impact the temperature field.

Imaging the mass transport was then possible using transmission FTIR spectroscopy. The experimental setup and the image processing methodology enabled us to measure the diffusion between two fluids even if they have similar IR spectral signatures. The results obtained in this study prove that transmission IR spectroscopy is a versatile tool to quantitatively investigate the mass transport in microfluidic chips in a very short period (on the order of ten seconds to record a multispectral image). The fast acquisition opens possibilities for this technique to observe transient phenomena.

Higher temperatures could have been investigated by optimizing the microfluidic device design to overcome degassing. However, even with a narrow range of temperatures, it was demonstrated that diffusion coefficient increases with temperature, as predicted by the Stokes-Einstein relationship. Such measurements were performed with high control of the uncertainty and obtained for residuals < 5% compared to the model. These results pave the way toward advanced quasireal-time mass transfer characterization to better understand in situ phenomena in more complex systems using transmission FTIR spectroscopy.

Acknowledgments

The authors gratefully acknowledge the French National Research Agency (ANR) for its support through project I2MPAC, grant number ANR-20-CE05-0018-01. Mr K. Krause is gratefully acknowledged for his fruitful discussions during manuscript preparation. Mr T. Chavatte's help during the preparation of the temperature field measurements was deeply appreciated.

References

[1] Mark F Coughlin and Roger D Kamm. The Use of Microfluidic Platforms to Probe the Mechanism of Cancer Cell Extravasation. *Advanced Healthcare Materials*, 9(8):1901410, apr 2020.

[2] Andrew J. DeMello. Control and detection of chemical reactions in microfluidic systems. *Nature*, 442(7101):394–402, 2006.

[3] Zifei Yan, Jiaxin Tian, Chencan Du, Jian Deng, and Guangsheng Luo. Reaction kinetics determination based on microfluidic technology. *Chinese Journal of Chemical Engineering*, 41:49–72, 2022.

[4] Jean Baptiste Salmon and Armand Ajdari. Transverse transport of solutes between co-flowing pressure-driven streams for microfluidic studies of diffusion/reaction processes. *Journal of Applied Physics*, 101(7), 2007.

[5] George M. Whitesides. The origins and the future of microfluidics. *Nature*, 442(7101):368–373, 2006.

[6] William A. Braff, Martin Z. Bazant, and Cullen R. Buie. Membrane-less hydrogen bromine flow battery. *Nature Communications*, 4:1–6, 2013.

[7] Erik Kjeang. *Microfl uidic Fuel Cells and Batteries*. 2014.

[8] M. N. Nasharudin, S. K. Kamarudin, U. A. Hasran, and M. S. Masdar. Mass transfer and performance of membrane-less micro fuel cell: A review. *International Journal of Hydrogen Energy*, 39(2):1039–1055, 2014.

[9] Gianni Orsi, Mina Roudgar, Elisabetta Brunazzi, Chiara Galletti, and Roberto Mauri. Water-ethanol mixing in T-shaped microdevices. *Chemical Engineering Science*, 95:174–183, 2013.

[10] Christine Peters, Ludger Wolff, Sandra Haase, Julia Thien, Thorsten Brands, Hans Jürgen Koß, and André Bardow. Multicomponent diffusion coefficients from microfluidics using Raman microspectroscopy. *Lab on a Chip*, 17(16):2768–2776, 2017.

[11] Joëlle Aubin, Montse Ferrando, and Vladimir Jiricny. Current methods for characterising mixing and flow in microchannels. *Chemical Engineering Science*, 65(6):2065–2093, 2010.

[12] Reiko Kuriyama, Tomotaka Nakagawa, Kazuya Tatsumi, and Kazuyoshi Nakabe. Two-dimensional fluid viscosity measurement in microchannel flow using fluorescence polarization imaging. *Measurement Science and Technology*, 32(9):095402, sep 2021.

[13] Christopher T. Culbertson, Stephen C. Jacobson, and J. Michael Ramsey. Diffusion coefficient measurements in microfluidic devices. *Talanta*, 56(2):365–373, 2002.

[14] Jean Baptiste Salmon, Armand Ajdań, Patrick Tabeling, Laurent Servant, David Talaga, and Mathieu Joanicot. In situ Raman imaging of interdiffusion in a microchannel. *Applied Physics Letters*, 86(9):1–3, 2005.

[15] Adam F. Chrimes, Khashayar Khoshmanesh, Paul R. Stoddart, Arnan Mitchell, and Kourosh Kalantar-Zadeh. Microfluidics and raman microscopy: Current applications and future challenges. *Chemical Society Reviews*, 42(13):5880–5906, 2013.

[16] Takato Uema, Toshiya Ohata, Yutaka Washizuka, Ryo Nakanishi, Daisuke Kawashima, and Naoto Kakuta. Near-infrared imaging in a microfluidic channel of aqueous acid–base reactions. *Chemical Engineering Journal*, 403(July 2020):126338, 2021.

[17] Adeline Perro, Gwenaelle Lebourdon, Sarah Henry, Sophie Lecomte, Laurent Servant, and Samuel Marre. Combining microfluidics and FT-IR spectroscopy: Towards spatially resolved information on chemical processes. *Reaction Chemistry and Engineering*, 1(6):577–594, 2016.

[18] Yukihiro Ozaki. Infrared Spectroscopy—Mid-infrared, Near-infrared, and Far-infrared/Terahertz Spectroscopy. *Analytical Sciences*, 37(9):1193–1212, sep 2021.

[19] Hiroki Yamashita, Naoto Kakuta, Daisuke Kawashima, and Yukio Yamada. Measurement of temperature-dependent diffusion coefficients of aqueous solutions by near-infrared simultaneous imaging of temperature and concentration. *Biomedical Physics and Engineering Express*, 4(3), 2018.

[20] K L.Andrew Chan and Sergei G Kazarian. FT-IR spectroscopic imaging of reactions in multiphase flow in microfluidic channels. *Analytical Chemistry*, 84(9):4052–4056, 2012.

[21] S. Chevalier, J.-N. Tourvieille, A. Sommier, and C. Pradère. Infrared thermospectroscopic imaging of heat and mass transfers in laminar microfluidic reactive flows. *Chemical Engineering Journal Advances*, 8:100166, nov 2021.

[22] Andrew V. Ewing, Graham S. Clarke, and Sergei G. Kazarian. Attenuated total reflection-Fourier transform infrared spectroscopic imaging of pharmaceuticals in microfluidic devices. *Biomicrofluidics*, 10(2):024125, mar 2016.

[23] L. G. Longsworth. Temperature Dependence of Diffusion in Aqueous Solutions. *The Journal of Physical Chemistry*, 58(9):770–773, sep 1954.

[24] Houssein Ammar, Bertrand Garnier, Ahmed Ould el Moctar, Hervé Willaime, Fabrice Monti, and Hassan Peerhossaini. Thermal analysis of chemical reactions in microchannels using highly sensitive thin-film heat-flux microsensor. *Chemical Engineering Science*, 94:150–155, 2013.

[25] Guilhem Velve Casquillas, Chuanhai Fu, Le Berre, Jeremy Cramer, Sebastien Meance, Adrien Plecis, Damien Baigl, Jean-jacques Greffet, Yong Chen, and Phong T Tran. Fast microfluidic temperature control for high resolution live cell imaging. *Lab on a Chip*, pages 484–489, 2011.

[26] Vincent Miralles, Axel Huerre, Florent Malloggi, and Marie-caroline Jullien. A Review of Heating and Temperature Control in Microfluidic Systems: Techniques and Applications. *Diagnostics*, pages 33–67, 2013.

[27] Monpichar Srisa-Art and Yuji Furutani. Simple and rapid fabrication of PDMS microfluidic devices compatible with FTIR microspectroscopy. *Bulletin of the Chemical Society of Japan*, 89(2):195–202, 2016.

[28] Stéphane Chevalier, Jean-Noël Tourvieille, Alain Sommier, Jean-Christophe Batsale, Bruno Beccard, and Christophe Pradère. Thermal Camera-Based Fourier Transform Infrared Thermospectroscopic Imager. *Applied Spectroscopy*, 75(4):462–474, apr 2021.

[29] Jukka Hietala, Antti Vuori, Pekka Johnsson, Pollari Ilkka, Werner Reutemann, and Heinz Kieczka. Formic acid. In B Elvers, editor, *Ullmann's Encyclopedia of Industrial Chemistry*, volume A12, pages 1–12. Wiley-VCH Verlag GmbH & Co, 2016.

[30] A. Aouali, S. Chevalier, A. Sommier, E. Abisset-Chavanne, J. C. Batsale, and C. Pradere. 3D infrared thermospectroscopic imaging. *Scientific Reports*, 10(1):1–11, 2020.

[31] Andrew Evan Kamholz, Bernhard H. Weigl, Bruce A. Finlayson, and Paul Yager. Quantitative analysis of molecular interaction in a microfluidic channel: The T-sensor. *Analytical Chemistry*, 71(23):5340–5347, 1999.

[32] Thomas Gervais and Klavs F. Jensen. Mass transport and surface reactions in microfluidic systems. *Chemical Engineering Science*, 61(4):1102–1121, 2006.

[33] C. Pradere, C. Hany, J. Toutain, and J. C. Batsale. Thermal analysis for velocity, kinetics, and enthalpy reaction measurements in microfluidic devices. *Experimental Heat Transfer*, 23(1):44–62, 2010.

[34] Thomas Lafargue-Tallet, Romain Vaucelle, Cyril Caliot, Abderezak Aouali, Emmanuelle Abisset-Chavanne, Alain Sommier, Raymond Peiffer, and Christophe Pradere. Active thermo-reflectometry for absolute temperature measurement by infrared thermography on specular materials. *Scientific Reports*, 12(1):1–19, 2022.

[35] L. A. Dunn and R. H. Stokes. The diffusion of monocarboxylic acids in aqueous solution at 25°. *Australian Journal of Chemistry*, 18(3):285–296, 1965.

[36] W. J. Albery, A. R. Greenwood, and R. F. Kibble. Diffusion coefficients of carboxylic acids. *Transactions of the Faraday Society*, 63:360–368, 1967.

[37] Iago Pereiro, Anna Fomitcheva Khartchenko, Lorenzo Petrini, and Govind V. Kaigala. Nip the bubble in the bud: A guide to avoid gas nucleation in microfluidics. *Lab on a Chip*, 19(14):2296–2314, 2019.

[38] J. Mikael Karlsson, Muriel Gazin, Sanna Laakso, Tommy Haraldsson, Surbhi Malhotra-Kumar, Minna Mäki, Herman Goossens, and Wouter Van Der Wijngaart. Active liquid degassing in microfluidic systems. *Lab on a Chip*, 13(22):4366–4373, 2013.

[39] Eric H. Oelkers. Calculation of diffusion coefficients for aqueous organic species at temperatures from 0 to 350 °C. *Geochimica et Cosmochimica Acta*, 55(12):3515–3529, 1991.

[40] M. Lehtihet, E. Abisset, S. Chevalier, A. Sommier, C. Pradere, and J. Leng. Thermospectroscopic infrared imaging of a confined drying process. *Chemical Engineering Journal*, 403(April 2020):126167, jan 2021.

[41] John Crank. *The Mathematics of Diffusion*. Oxford University Press, 2nd edition.

[42] Kevin Roger, Omer Atasi, and Benjamin Lalanne. Measuring mutual diffusion coefficients in aqueous binary mixtures with unidimensional drying cells. *Physical Chemistry Chemical Physics*, 25(2):994–998, 2023.

[43] Ayanjeet Ghosh, Arnaldo L. Serrano, Tracey A. Oudenhoven, Joshua S. Ostrander, Elliot C. Eklund, Alexander F. Blair, and Martin T. Zanni. Experimental implementations of 2D IR spectroscopy through a horizontal pulse shaper design and a focal plane array detector. *Optics Letters*, 41(3):524, feb 2016.